Journal Pre-proofs

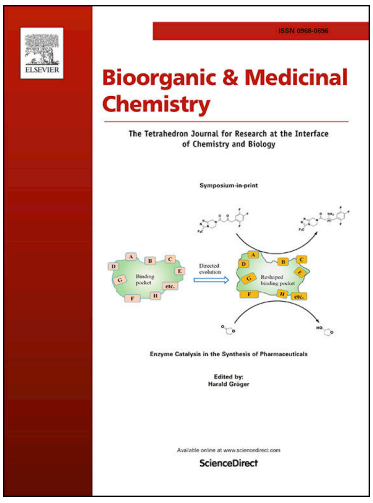

YAT2150: Overcoming limitations of traditional amyloid dyes in aggregation studies

Irene Álvarez-Berbel, Salomé Llabrés, Òscar Domènech, Maria Antonia Busquets, Xavier Fernàndez-Busquets, Elsa M. Arce, Rosalina Gavín, José Antonio del Río, Diego Muñoz-Torrero, FJavier Luque, Raimon Sabate, Alba Espargaró

PII: S0968-0896(25)00104-X
DOI: https://doi.org/10.1016/j.bmc.2025.118163
Reference: BMC 118163

To appear in: *Bioorganic & Medicinal Chemistry*

Received Date: 31 December 2024
Revised Date: 7 March 2025
Accepted Date: 17 March 2025

Please cite this article as: I. Álvarez-Berbel, S. Llabrés, O. Domènech, M.A. Busquets, X. Fernàndez-Busquets, E.M. Arce, R. Gavín, J.A. del Río, D. Muñoz-Torrero, F. Luque, R. Sabate, A. Espargaró, YAT2150: Overcoming limitations of traditional amyloid dyes in aggregation studies, *Bioorganic & Medicinal Chemistry* (2025), doi: https://doi.org/10.1016/j.bmc.2025.118163

YAT2150: Overcoming limitations of traditional amyloid dyes in aggregation studies

Irene Álvarez-Berbel[1], Salomé Llabrés[1,2], Òscar Domènech[1,3], Maria Antonia Busquets[1,4], Xavier Fernàndez-Busquets[3,5,6], Elsa M. Arce[7], Rosalina Gavín[8,9,10,11], José Antonio del Río[8,9,10,11], Diego Muñoz-Torrero[4,7], F Javier Luque[2,4,12], Raimon Sabate[1,4,*], Alba Espargaró[1,4,*]

[1]Department of Pharmacy and Pharmaceutical Technology and Physical-Chemistry, Faculty of Pharmacy and Food Sciences, University of Barcelona, Av. Joan XXIII, 27-31, 08028-Barcelona, Spain.

[2]Institute of Theoretical and Computational Chemistry (IQTCUB), University of Barcelona, Spain.

[3]Institute of Nanoscience and Nanotechnology (IN^{2}UB), University of Barcelona, Spain.

[4]Institute of Biomedicine (IBUB), University of Barcelona, Spain.

[5]Barcelona Institute for Global Health (ISGlobal), Hospital Clínic-Universitat de Barcelona, Barcelona, Spain

[6]Institute for Bioengineering of Catalonia (IBEC), The Barcelona Institute of Science and Technology, Barcelona, Spain

[7]Laboratory of Medicinal Chemistry, Faculty of Pharmacy and Food Sciences, University of Barcelona, Av. Joan XXIII, 27-31, 08028-Barcelona, Spain.

[8]Department of Cell Biology, Physiology and Immunology, Faculty of Biology, University of Barcelona, Av. Diagonal, 643, Les Corts, 08028-Barcelona, Spain.

[9]Molecular and Cellular Neurobiotechnology, Institute for Bioengineering of Catalonia, Barcelona, Spain.

[10]Institute of Neuroscience, University of Barcelona, Barcelona, Spain.

[11]Center for Networked Biomedical Research in Neurodegenerative Diseases (CIBERNED), Barcelona-Madrid, Spain.

[12]Department of Nutrition, Food Sciences, and Gastronomy, Faculty of Pharmacy and Food Sciences, University of Barcelona, Prat de la Riba 171, 08921-Santa Coloma de Gramenet, Spain.

* Corresponding author: *E-mail address:* rsabate@ub.edu (R Sabate), aespargaro@ub.edu (A Espargaró)

Keywords: amyloid; aggregation; YAT2150; inclusion bodies; amyloid inhibitor; screening

Abstract:

Amyloid fibrils, which are aggregates of misfolded proteins characterized by β-sheet-rich structures, are implicated in several neurodegenerative and systemic pathologies, including Alzheimer's and Parkinson's diseases and type II diabetes mellitus. Traditional amyloid markers, such as Congo Red and Thioflavin T, are widely used for amyloid detection but present limitations, particularly in cellular assays, due to spectral interference and aggregation inhibition. This study investigates YAT2150, a novel fluorescent dye with enhanced amyloid-binding specificity and sensitivity, as a potential alternative to conventional dyes. We evaluated YAT2150's efficacy for detecting amyloid aggregates in both *in vitro* and *in cellula* assays. First, we compared its fluorescence intensity and binding specificity to that of Thioflavin T in amyloid fibril assays, demonstrating that YAT2150 exhibits high affinity and selectivity for amyloid structures, with minimal interference from non-aggregated proteins. Furthermore, we explored YAT2150's utility in *Escherichia coli* as a model system for studying protein aggregation and amyloid formation in a procaryotic cellular context. Our findings indicate that YAT2150 effectively labels amyloid-like inclusion bodies in *E. coli*, producing a robust fluorescence signal with low background noise. These results suggest that YAT2150 is a promising new tool for amyloid research, offering greater sensitivity compared to traditional dyes, even in complex cellular environments.

1. INTRODUCTION

Protein misfolding and aggregation into amyloid structures are associated with an increasing number of human diseases, collectively known as amyloidoses. These range from neurodegenerative pathologies like Alzheimer's and Parkinson's diseases to non-neurodegenerative amyloidoses, such as type II diabetes mellitus [1]. The aggregation of misfolded proteins into highly ordered, insoluble β-sheet-rich structures is a hallmark of these disorders, contributing directly to their pathology [2]. The link between amyloid formation and disease has made amyloid structures a crucial target for therapeutic intervention in what are collectively termed "conformational diseases". With the rising global population and increased life expectancy, these disorders are projected to pose significant public health challenges, making the development of new strategies to prevent or treat amyloid aggregation a high priority in biomedical research.

The characteristic β-cross-linked conformation in which individual β-strands run perpendicular to the fibril axis [1] can be detected using specific dyes such as Congo Red (CR), Thioflavin T (ThT) and

Thioflavin S (ThS) [3–5]. However, these traditional amyloid markers have limitations in therapeutic research. CR has amyloid-inhibiting properties that can interfere with real-time monitoring of aggregation [6] and ThT fluorescence overlaps with cellular constituents with intrinsic fluorescence properties and aromatic compounds [7]. ThS offers better membrane permeability than ThT but suffers from similar spectral interference issues [5]. These shortcomings underscore the need for alternative tools that can better serve in both research and therapeutic studies of amyloid diseases.

Recently, a new dye capable of detecting amyloid structures called YAT2150 (**Figure 1**), the active component of the commercial protein aggregation detection reagent ProteoStat® [8], has been reported. In the presence of amyloid aggregates, YAT2150 emits an intense red fluorescence at ~ 600 nm when excited at ~ 500 nm. Compared to Thioflavins, YAT2150 does not have the limitations mentioned above and exhibits higher fluorescence intensity; therefore, it could represent an advantage in studies of amyloid aggregation [9].

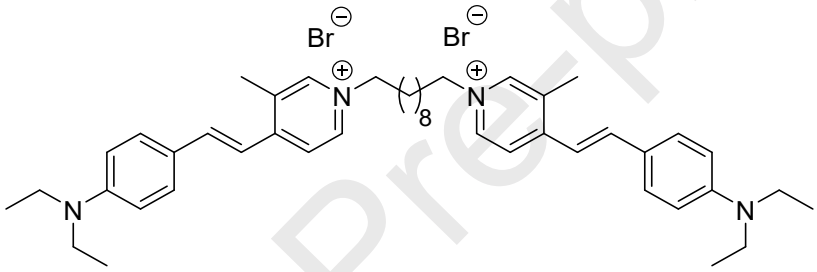

Figure 1. Chemical structure of YAT2150

Many approaches exist to characterize amyloid aggregation *in vitro* [10,11]. Unfortunately, *in vitro* results often cannot be reproduced when tested *in cellula* or *in vivo* due to the complex cellular environment. Animal models, however, are highly complex and expensive, which is inefficient in the early stages of research. In this context, bacteria have emerged as a simple, inexpensive and, above all, physiologically relevant system for studying amyloid aggregation and anti-amyloid compounds [12,13]. *Escherichia coli* is widely used in the biotechnology industry as a factory to produce recombinant peptides and proteins due to (a) its rapid growth; (b) the ability to achieve high cell density cultures; (c) the use of simple and inexpensive culture media; and (d) the rapid and easy transformation with exogenous DNA [14]. However, the continuous expression of recombinant proteins overwhelms cellular quality control mechanisms, resulting in misfolded proteins that accumulate and form intracellular aggregates called inclusion bodies (IBs). Recombinant protein in IBs can vary from 50% of the total protein in early stages of aggregation to more than 90% in mature IBs [15]. It is now widely accepted that much of the protein in IBs has an amyloid conformation and thus can be detected by amyloid-specific dyes [16–19]. The tendency of amyloid-prone proteins to aggregate in bacteria has

made them an outstanding model for studying the mechanisms of amyloid formation and has driven the search for inhibitors targeting numerous proteins associated with human diseases [13,20]. In this context, this work aims to study the applicability of the novel YAT2150 as an alternative dye for detecting and monitoring amyloid formation *in vitro* and *in cellula*.

2. MATERIALS AND METHODS

2.1. Reagents: The YAT2150 dye and the amyloid aggregation pan-inhibitor DP-128 were prepared as previously reported [8,21]. Both compounds were dissolved in dimethyl sulfoxide (DMSO, CAS 67-68-5) and stored at 4 °C until use.

Model proteins, including bovine serum albumin (BSA, CAS 9048-46-8), lysozyme (CAS 12650-88-3), and insulin (CAS 11061-68-0) were obtained from Merck, while the amyloid beta 1-40 (Aβ40, CAS 131438-79-4) peptide was purchased from Bachem. The HET-s prion-forming domain of *Podospora anserina* (HET-s PFD) [22], along with yeast prions Sup35 and Ure2p [23], and full-length vole prion protein (vPrP) [24], were produced recombinantly. Amylin core sequences (wild-type, reverse, and scrambled) were obtained from EZ Biolab, Inc. (Carmel, IN) [25].

Isopropyl-β-D-1-thiogalactopyranoside (IPTG, CAS 367-93-1) was obtained from Apollo Scientific and diluted in Milli-Q water (MQ-H2O). ThT (CAS 2390-54-7) and ThS (CAS 1326-12-1), as well as antibiotics such as kanamycin (CAS 70560-51-9), ampicillin (CAS 69-52-3), and chloramphenicol (CAS 56-75-7), were purchased from Sigma-Aldrich. All antibiotics and chemicals were dissolved in MQ-H_2O except for chloramphenicol, which was dissolved in methanol (CAS 67-56-1). Aliquots of IPTG and antibiotics were stored at -20 °C, while ThT and ThS were kept at room temperature, protected from light.

The minimal medium M9 contained in 100 mL: 10 mL M9 salts 10× (0.68 g Na_2HPO_4 (CAS 7558-79-4), 0.30 g KH_2PO_4 (CAS 7778-77-0), 0.05 g NaCl (CAS 7647-14-5) and 0.10 g NH_4Cl (CAS 12125-02-9)), 0.2 mL 1 M $MgSO_4$ (CAS 7487-88-9), 0.2 mL 50 mM $CaCl_2$ (CAS 10043-52-4), 2.0 mL 20% glucose (CAS 50-99-7) and 87.6 mL MQ-H_2O.

2.2. Monomeric Aβ40 preparation: 1 mg of Aβ40 was dissolved in 500 µL of Hexafluoro-2-propanol (HFIP, CAS 920-66-1) while being vigorously stirred at room temperature for 1 h. The solution was sonicated for 30 min and then stirred for an additional hour at room temperature. Afterward, the solution was cooled at 4 °C for 30 min to prevent solvent evaporation during aliquot collection. Samples were filtered through 0.22 µm filters to remove any insoluble material. Finally, aliquots of Aβ40 were collected, and HFIP was evaporated under a gentle nitrogen stream. The monomeric Aβ40 aliquots were stored at -20 °C.

2.3. *In vitro* aggregation: BSA was prepared at 0.5 mg·mL^{-1} in 20 mM Tris-HCl (CAS 1185-53-1) (pH 7.4) [26], lysozyme at 0.5 mg·mL^{-1} in 10 mM HCl (CAS 7647-01-0) (pH 2) [27], and insulin at 0.5 mg·mL^{-1} in 50 mM NaCl (pH 1.6, adjusted with HCl) [28]. Monomeric Aβ40 was dissolved in 50 µL DMSO, sonicated for 10 min, and then diluted in Native Buffer (NB: 50 mM Tris and 150 mM NaCl, pH 7.4) to a final concentration of 15 µM. For HET-s PFD, three different sample conditions were prepared by dissolving 200 µM of the protein: (1) in buffer A (0.2 M anhydrous boric acid (CAS 1303-86-2), 0.05 M citric acid monohydrate (CAS 5949-29-1), 0.03 M NaCl) or 20 mM acetic acid (CAS 64-19-7) at pH 2-3, (2) in a 1:1 ratio of buffer A and buffer B (20 mM trisodium phosphate dodecahydrate, CAS 10101-89-0) at pH 7 (low ionic strength), and (3) in 200 mM acetic acid and 1 M Tris-HCl at pH 7 (high ionic strength). Aggregation of vPrP was initiated after transferring the protein to a NB. Fiber formation for Sup35 and Ure2p was performed at 10 µM concentration in NB. Wild-type, reverse and scrambled amylin (WT-, R- and S-amylin, respectively) were reconstituted in 50 µL of DMSO, sonicated for 10 minutes, then diluted with 100 µL of 100 µM acetate buffer (pH 5.5) and 850 µL of ultrapure water to achieve a final peptide concentration of 100 µM. All samples were incubated at 37 ºC and 1400 rpm in a Thermomixer (Eppendorf) until aggregation, except for BSA, lysozyme and insulin, which were incubated at 65 ºC. Control samples were stored at 4 °C without incubation to serve as unaggregated controls. After incubation, 1M Tris-HCl (pH 8.0) was added to the acidic samples at a 1:1 ratio.

2.4. *In vitro* inhibition of Aβ40 aggregation: The aggregation of Aβ40 (15 µM) in the absence and presence of DP-128 inhibitor at different concentrations (10 and 100 µM) was monitored by determining the fluorescence signal of 2 µM YAT2150, which was present from the start of the incubation, using a CLARIOstar plate reader (BMG LABTECH). Kinetic measurements were performed by incubating the samples at 37 °C with shaking at 700 rpm, with fluorescence readings taken every 300 seconds for 24 h. After the incubation period, the fluorescence spectrum following aggregation was recorded using an Aminco Bowman Series 2 fluorometer (SLM Aminco).

2.5. Microscopy techniques for amyloid characterization:

2.5.1. Atomic force microscopy (AFM): For AFM studies, 2 µL of sample were incubated on a freshly cleaved mica disc and let to adsorb for 2 min. Afterwards, mica disc was gently rinsed with milliQ water to remove non-adsorbed sample and dried under a nitrogen stream. AFM samples were scanned with a multimode Nanoscope IV from Digital Instruments (Bruker, AXS Co., Madison, WI, USA) on air and in intermittent contact mode with RTESPA-150 probes, with a nominal spring constant of 5 nN nm^{-1} and a nominal radius of 8 nm, from Bruker AFM probes (Camarillo, CA, USA). All images were

processed by NanoScope Analysis Software (Bruker AXS Corporation, Madison, WI, USA).

2.5.2. Electron Microscopy: For negative staining, the samples were adsorbed onto freshly glow-discharged, carbon-coated grids, then rinsed with water and stained using 1% (w/v) uranyl acetate. To ensure optimal particle size, both bundle samples and disordered fibrils formed at pH 7 were typically sonicated briefly (5 seconds using a Kontes sonicator at approximately 60 W). Micrographs were captured using a Philips CM120 microscope.

2.6. *In cellula* aggregation: Assays were performed using *E. coli* overexpressing Aβ42, human α-synuclein (α-SynH), HET-s PFD and Ure2p. Competent *E. coli* BL21(DE3) cells were transformed with the required vectors carrying the DNA sequence of the respective proteins. For bacterial culture preparation, a colony of BL21(DE3) cells carrying the plasmid to be expressed was inoculated into 10 mL M9 minimal medium containing 50 μg mL^{-1} kanamycin, 100 μg mL^{-1} ampicillin and/or 12.5 μg mL^{-1} chloramphenicol (depending on the vector used), at 37 ºC. A sufficient amount of culture was transferred to a fresh M9 medium with the corresponding antibiotic(s) and incubated at 37 °C and 250 rpm. When an OD_{600} of 0.5-0.6 was reached, 200 μL culture was transferred to a 1.5 mL Eppendorf tube with 790 μL induced M9 medium (containing 10 μL IPTG 100 mM) and 200 μL to another tube with 790 μL non-induced M9 medium (without IPTG). Then, 10 μL YAT2150 was added to a final concentration of 2 μM. The process was repeated using ThS at a final concentration of 25 μM. Samples were incubated at 37 °C and 250 rpm for 24 h. Fluorescence was determined with a CLARIOstar (BMG LABTECH). Additionally, OD_{600} was determined in a DTX 800 multimode reader (Beckman Coulter) to normalise fluorescence based on bacterial concentration.

2.7. *In cellula* inhibition of Aβ42 aggregation and kinetics analysis: Building on the *in cellula* aggregation protocol mentioned above, DP-128 was added as inhibitor of amyloid aggregation at 5, 10 and 20 μM to test the ability of YAT2150 to determine the action of potential amyloid inhibitors. For kinetic and thermodynamic parameters, amyloid aggregation was approached mathematically as an autocatalytic reaction using a previously described equation [13,29].

2.8. Determination of relative fluorescence: Fluorescence resulting from the binding of the different dyes to model proteins (*in vitro*) or IBs (*in cellula*) was determined using an Aminco Bowman Series 2 spectrofluorimeter (SLM Aminco) and a CLARIOstar (BMG LABTECH). Excitation and emission wavelengths were set at λ_{ex} = 465 nm and λ_{em} = 595 nm for YAT2150; λ_{ex} = 445 nm and λ_{em} = 485 nm for ThT; and λ_{ex} = 440 nm and λ_{em} = 485 nm for ThS.

2.9. Fluorescence microscopy in bacteria: Bacterial cells overexpressing Aβ42 and HET-s PFD were

incubated for 1 h with 2 μM YAT2150. Following incubation, excess YAT2150 was removed by centrifugation, and the cells were resuspended in PBS and placed on a microscope slide for imaging. Images were acquired using LED light with a CYR70010 filter, or with phase contrast, using a Leica Thunder microscope equipped with an sCMOS camera (Leica K5). All imaging was performed at the Centres Científics i Tecnològics of the Universitat de Barcelona (CCiTUB).

2.10. Molecular modelling of the binding mode of YAT2150 to Aβ40 fibrils:

2.10.1. Molecular docking calculations of YAT2150 on Aβ40 fibrils.

The two-fold extended morphology of Aβ40 fibrils (PDB id 6W0O [30]) was considered for docking calculations. The 6-monomer long fibrils were modelled from the structures included in the protein data bank (PDB) (accounting for a total of 12 monomers). Protonation states were predicted using PropKa [31] and further checked by visual inspection. Due to the symmetrical structure of YAT2150, docking calculations were performed to identify the putative binding sites of the YAT2150 styryl-pyridinium moiety (i.e., the 3-methyl-4-[4-(diethylamino)styryl]-*N*-methylpyridinium moiety) present in YAT2150 using the open-source software rDock [32]. A total of 200 binding poses were recovered and filtered by their docking score (SCORE.INTER < -16 kcal/mol). Three binding modes were then selected by visual inspection and subjected to Molecular Dynamics simulations to assess their stability.

2.10.2. System Setup of YAT2150 bound to Aβ40 fibrils.

The structural integrity of the three binding modes was examined building up Aβ40-YAT2150 complexes consisting of the YAT2150 styryl-pyridinium moiety simultaneously bound at the three binding sites in the modelled Aβ40 fibril. This system includes 12 fibrils and three YAT2150 styryl-pyridinium units. The complexes were then solvated using a dodecahedral box of TIP3P water molecules accounting for a 12 Å spacing between the protein and the box edge, leading to a total of ~106,000 atoms. Counterions (Na^+) were added to maintain the neutrality of the simulated systems. Finally, three independent MD simulations were run to check the structural integrity of the YAT2150 styryl-pyridinium unit in the distinct sites of Aβ40.

The binding of the whole chemical skeleton of YAT2150 to Aβ40 fibrils in the most favourable pose as determined from previous studies required a larger protein model. Therefore, we extended the fibrils up to 11 monomers (accounting for a total of 22 monomers). Two styryl-pyridinium moieties were placed in the binding sites located at 10.5 Å, which gives enough space to include the decamethylene chain that bridges the two styryl-pyridinium units. Then, the systems were solvated using a

dodecahedral box of TIP3P water molecules accounting for a 12 Å spacing between the protein and the box edge. Counterions (Na^+) were added to maintain the neutrality of the simulated system. In total, the simulation system accounted for a total of ~127,000 atoms.

The amberff14sb force field [33] was used for the protein, Joung and Cheatham III parameters were used for the counterions [34], and the TIP3P model was used for the solvent [35]. Partial atomic charges for the YAT2150 styryl-pyridinium moiety and the whole YAT2150 were derived using the RESP protocol at the HF/6-31G(d) level of theory, as calculated with Gaussian09 [36].

2.10.3. Unbiased Molecular Dynamics simulations.

Each system was minimized using 4,000 steps of steepest descent, followed by 4,000 steps of conjugate gradient algorithm. Then, each system was gradually equilibrated in 6 steps. The systems were heated in the NVT ensemble from 100 to 300 K in three stages of 1 ns (100–150, 150–250, 250–300 K) with 5 $kcal \cdot mol^{-1}$ positional restraint on all the atoms of the protein and the ligand. Subsequently, the density of the system was equilibrated for 3 ns in the NPT ensemble (pressure: 1 bar, T: 300 K). During the last 2 ns of the equilibration run, the positional restraints were slowly released.

We performed three replicates of 100 ns-long production runs of the Aβ40-YAT2150(styryl-pyridinium) complexes to assess the stability of the predicted binding modes. The production runs of the YAT2150- Aβ40 complex with the whole YAT2150 were 500 ns long (three replicates, accounting for a total of 1.5 μs). All production runs were performed in the NPT ensemble, using a Langevin thermostat and a Montecarlo barostat to control temperature and pressure, respectively. SHAKE was applied to all bonds involving hydrogen atoms to allow for a time step of 2 fs, and all simulations were performed with the CUDA accelerated version of PMEMD implemented in the AMBER24 software [37]. To prevent the unfolding of the monomers at the edges of the fibrils, we applied soft positional restraints (1 $kcal \cdot mol^{-1}$) on the Cα atoms of the β sheets of each monomer.

3. RESULTS AND DISCUSSION

3.1. *In vitro* detection of amyloid fibres

3.1.1. Evaluation of YAT2150 binding capacity

BSA, lysozyme, and insulin were selected as model proteins to evaluate the binding capacity of YAT2150 to amyloid structures. These proteins form amyloid-like aggregates [26–28], making them suitable for studying amyloid-specific binding and hence to assess the performance of YAT2150

as amyloid marker. ThT, one of the most used amyloid dyes, was employed as a control. **Figure 2** illustrates that the different fluorescence spectra revealed maxima at ~ 595 nm for YAT2150 and ~ 480 nm for ThT in the presence of amyloid aggregates. Across all samples, aggregated proteins displayed higher fluorescence intensities compared to their non-aggregated counterparts, demonstrating the ability of YAT2150 to bind amyloid aggregates.

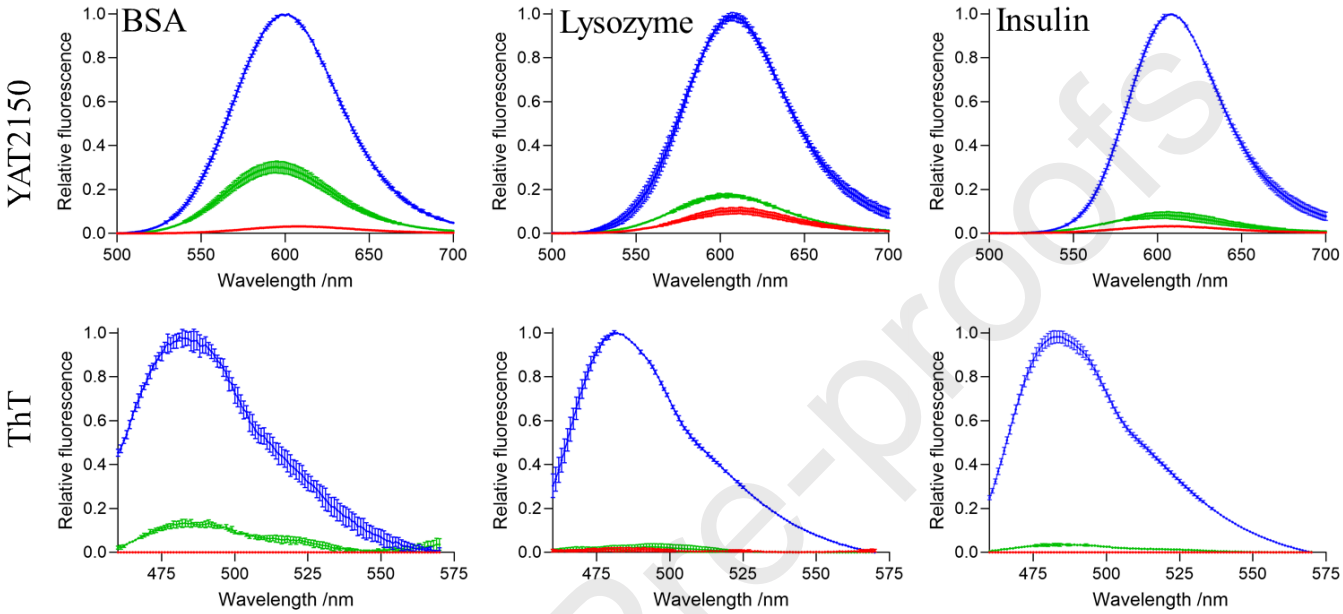

Figure 2. Detecting protein aggregation with YAT2150 and ThT. Fluorescence spectra of YAT2150 (top panel) and ThT (bottom panel) for aggregated (blue) and non-aggregated (green) BSA, lysozyme, and insulin. Negative controls (red) include YAT2150 or ThT.

As shown in **Figure 2**, both ThT and YAT2150 exhibit significant increases in fluorescence upon binding to amyloid structures in all three model proteins. Additionally, a slight shift in the emission maximum is observed for both dyes when comparing the spectra of amyloid structures (blue spectra) with those of non-aggregated proteins (green spectra). However, as previously reported, these slight shifts are of low relevance in the case of ThT due to the nature of its fluorescence enhancement [38]. In this context, **Figure 3** shows that when several amyloid-prone proteins are tested, ThT exhibits negligible shifts, whereas YAT2150 demonstrates a distinct hypochromic shift of ~4 nm for certain amyloid proteins, particularly in the spectra of vPrP and Ure2p. These shifts may be attributed to the dye's sensitivity to the molecular environment created by different structures, including restrictions in molecular motion, changes in polarity, or variations in the hydrophobicity of the surroundings, as previously described for dyes such as DMN [39].

3.1.2. Broad detection capabilities of YAT2150 across diverse amyloid-prone proteins

After confirming that YAT2150 specifically binds to various amyloid structures formed by the selected protein models, we expanded the study by assessing its detection capabilities using a diverse set of amyloid-prone proteins. These included the vPrP, the yeast prion-like proteins Sup35 and Ure2p, and different sequences of amylin, a peptide hormone implicated in type II diabetes mellitus [25]. As shown in **Figure 3**, YAT2150 successfully detected amyloid fibrils formed by amylin core sequences WT, R, and S, vPrP, Sup35, and Ure2p. Notably, the emission intensity of ThT varied significantly depending on the protein tested (for instance, high intensity for Sup35 and very low intensity for vPrP and Ure2p). In contrast, YAT2150 detected aggregates of all tested proteins, including vPrP and Ure2p, demonstrating broader applicability than ThT in amyloid monitoring.

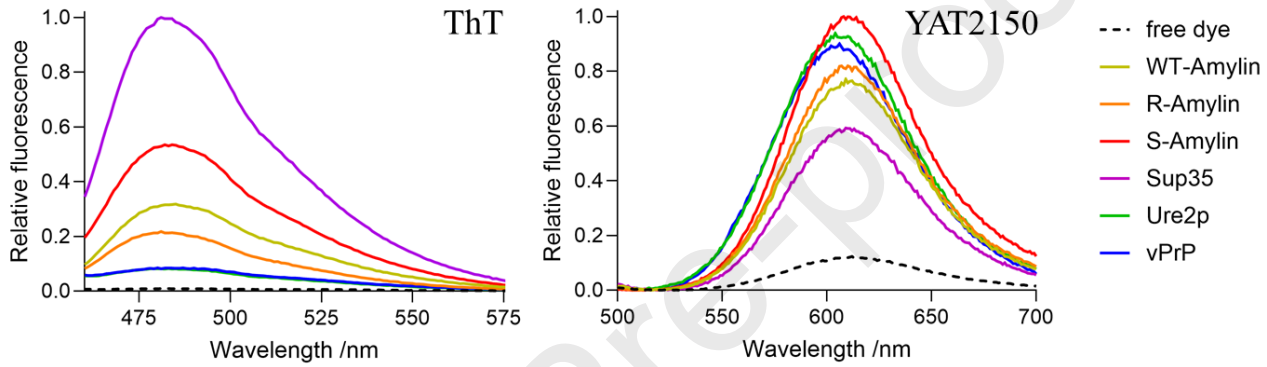

Figure 3. **Broad detection of protein fibres.** Emission spectra of ThT (25 µM; left) and YAT2150 (2 µM; right) after 5-min incubation at room temperature with fibres of different proteins. [Protein] = 20 µM; PBS pH 7.4.

The HET-s PFD is an excellent model for studying the binding capacity of YAT2150. It is well established that HET-s PFD fibrils exhibit different amyloid structures when aggregated, *in vitro*, under varying conditions, such as pH and salt concentration. Here, we analyzed three different amyloid conformational polymorphs of HET-s PFD that displayed different ThT fluorescence patterns depending on the aggregation conditions [22]. At pH 2, twisted fibres, primarily composed of three individual filaments and displaying a strong ThT signal (ThT+), are formed. In contrast, at pH 7, different morphologies are observed depending on ionic strength: bundled/stacked fibrils at high ionic strength and short fibrils in apparently amorphous/disordered groupings at low ionic strength (**Figure S1**). However, none of these pH 7 aggregates are detectable with ThT (ThT-) (**Figure 4**, left panel). Similarly, YAT2150 showed increased fluorescence for aggregates formed under acidic conditions. Notably, YAT2150 demonstrated an advantage over ThT by detecting HET-s PFD fibrils formed at pH 7 under high ionic strength conditions. However, like ThT, YAT2150 showed poor sensitivity in detecting aggregates formed at pH 7 with low ionic strength (**Figure 4**, right panel). This reduced

sensitivity may be attributed to the apparently amorphous nature of the aggregates formed under these conditions, which tend to have shorter, more compact fibrils, limiting dye-aggregate binding (**Figure S1**) [22]. These results suggest that ThT and YAT2150 have different binding modes.

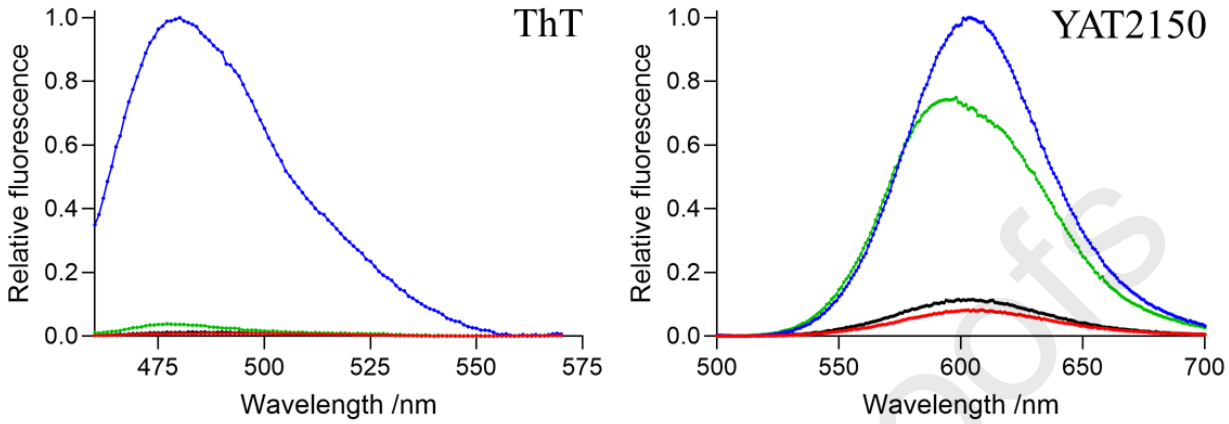

Figure 4. **Detection of HET-s PFD morphological variants.** Fluorescence spectra of ThT (left panel) and YAT2150 (right panel) for HET-s PFD in three morphological forms: triplet fibres formed at pH 2-3 (blue), single-stacked fibres aggregated at pH 7 at high ionic strength (green), and fibres with amorphous appearance aggregated at pH 7 at low ionic strength (black). In red, negative controls with YAT2150 or ThT.

3.1.3. Characterization of YAT2150 binding to Aβ1-40 fibrils

Aβ40, which is closely associated with Alzheimer's disease progression, was selected to gain further insight into the interaction of YAT2150 with amyloid proteins. In this study, we used Aβ40 fibrils, confirmed as ThT+ (**Figure 5a**), to evaluate the binding characteristics of YAT2150. Considering the emission data of free and Aβ-bound dye (B_{max}) using the one-site binding model (saturation binding curve, Eq. (1)):

$$y = \frac{B_{max} \cdot x}{K_d + x} \quad (1)$$

where y is the concentration of YAT2150 bound to Aβ40, and x is the dye concentration. The resulting saturation binding curve (**Figure 5b**) yielded a K_d value of 0.026 µM and a B_{max} of 0.592 µM. The low K_d suggests a high affinity of YAT2150 for Aβ40, indicating that the dye binds effectively to Aβ40 even at low concentrations. The B_{max}, representing the concentration at which the available Aβ40 binding sites are saturated by YAT2150, indicates a binding stoichiometry of 1:17 YAT2150:Aβ40. Together, these values indicate that YAT2150 binds with high affinity and specificity to Aβ40.

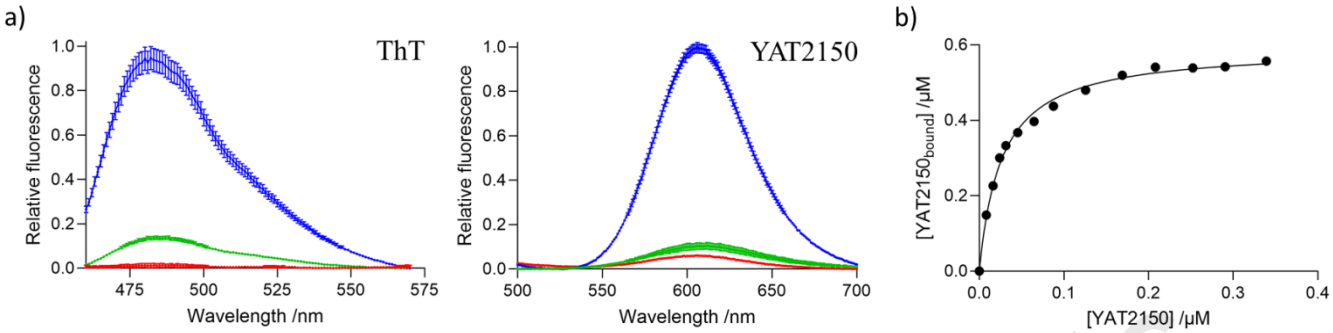

Figure 5: Detection and binding characterization of Aβ40 aggregation. a) Fluorescence spectra of ThT (left panel) and YAT2150 (right panel) for aggregated (blue) and non-aggregated (green) Aβ40. Negative controls with YAT2150 or ThT are shown in red. b) One-site binding model of YAT2150 binding to Aβ40 at a concentration of 10 µM.

To explore the potential binding mode of YAT2150, we performed docking calculations of the YAT2150 styryl-pyridinium moiety on the two-fold extended fibril (PDB id 6W0O) morphology detected in AD patients [30], which is a common fold found in recent cryo-EM studies [40–42]. The analysis of the results led to the identification of three possible binding modes of the styryl-pyridinium unit (**Figure S2**) The stability of these docking poses was then assessed using 100 ns-long molecular dynamics simulations. Only one binding mode was stable in the three independent MD simulations. In this binding mode, the YAT2150 styryl-pyridinium unit binds to the two-fold extended Aβ40 fibrils at the interface between the two fibrils over the backbone of the H13 and H14 by interacting with the side chain of V12 and Q15 residues of one fibril and the negative charge of the C-terminal acid of V40 of the other fibril and sporadically of the side chain of E11.

Based on these findings, we modelled the interaction between YAT2150 with a larger model of the Aβ40 fibril that includes 22 monomers (**Figure 6**). The initial model of YAT2150 retained the binding mode detailed above for its two styryl-pyridinium units. Accordingly, the two styryl-pyridinium moieties were separated 10.5 Å (distance between the N atoms of the pyridine rings). This model was then simulated for 500 ns using unbiased Molecular Dynamics simulations per triplicate. The binding mode of YAT2150 was stable during all the simulation time retaining all the interactions described above (**Figure S3**). YAT2150 binds to a groove at the interface between both fibrils, formed by the backbone of H13 and H14 and the side chains of V12 and Q15. Both styryl-pyridinium moieties establish van der Waals interactions with the V12 side chains and intermittent salt bridge interactions with the acid groups of the C-terminal end of V40 and the side chains of E11. The decamethylene linker establishes hydrophobic contacts with the V12 side chain. This hydrophobic environment allows the linker to adopt its extended form resulting in a distance between the two styryl-pyridinium units of 12.8

± 0.3 Å (averaged for the three independent MD simulations; **Figure S4**). Noteworthy, the stoichiometry of this binding mode is 1:16 YAT2150:Aβ40 monomers, in line with the experimental values reported in this work.

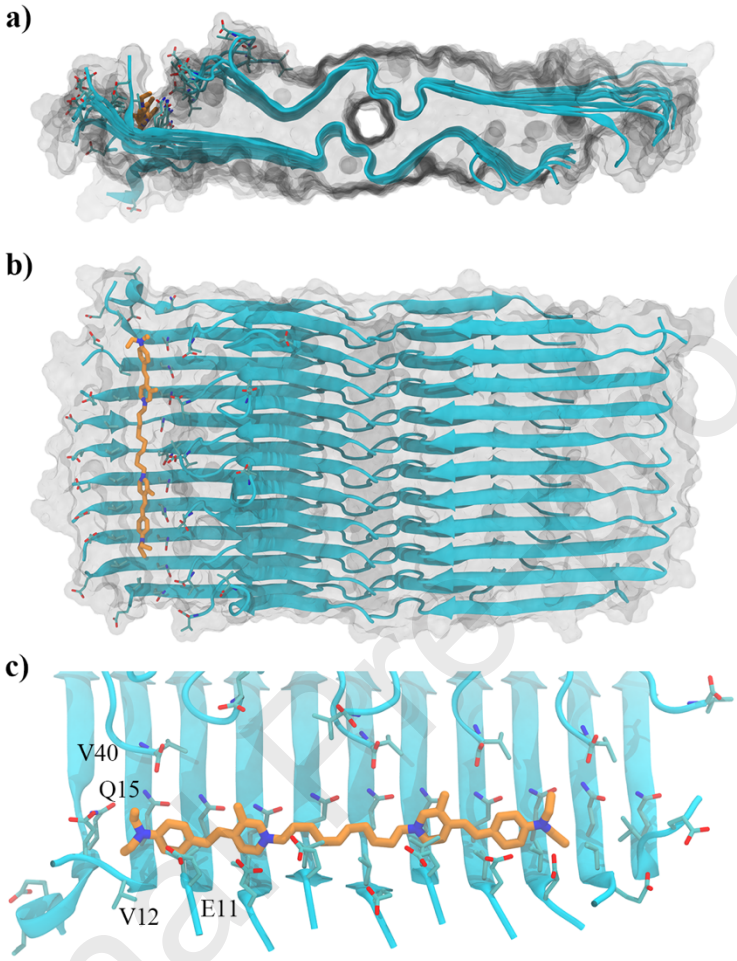

Figure 6. (a) Side view and (b) Top view of the proposed binding mode for YAT2150 to Aβ40 fibrils. (c) Close up view of the interactions between YAT2150 and the residues of Aβ40 fibrils (22 monomers). Aβ40 fibrils are represented as blue cartoon and the YAT2150 molecule is shown as orange sticks. Protein surface is shown as transparent grey surface.

The molecular docking and dynamics simulations performed in this study provide structural insight into the interaction of YAT2150, the active component of ProteoStat® [8], with amyloid fibrils. These findings align with the known mechanism of ProteoStat® as a molecular rotor dye [43], which remains non-fluorescent in solution due to free intramolecular rotation but becomes highly fluorescent upon binding to misfolded and aggregated proteins. The stabilization of YAT2150 within the amyloid fibril structure, as observed in our simulations, suggests that its restricted mobility within the cross-β spine inhibits rotation, thereby enhancing fluorescence.

3.1.4. *In vitro* real-time monitoring of amyloid aggregation kinetics and inhibition

In this study, we sought to demonstrate that YAT2150 not only detects amyloid aggregates at the final stage but also enables real-time monitoring of their formation kinetics. To achieve this, we tracked the aggregation kinetics of Aβ40 using YAT2150 in the absence and presence of the known amyloid pan-inhibitor DP-128 [44] at concentrations of 10 µM and 100 µM. Previously, we verified that DP-128 does not interfere with YAT2150 fluorescence by analysing the fluorescence spectrum of insulin fibrils labelled with YAT2150 before and after DP-128 addition. No changes were observed after 30 minutes of incubation, confirming the absence of interaction between DP-128 and YAT2150 (data not shown). As illustrated in **Figure 7**, the aggregation process follows a characteristic two-step autocatalytic sigmoidal curve, corresponding to nucleation and elongation phases. YAT2150 effectively monitored Aβ40 aggregation kinetics and demonstrated amyloid inhibition in the presence of DP-128; displaying inhibitions of 67.6 and 91.6% for 10 and 100 µM DP-128, respectively. Importantly, the inhibition percentages obtained with DP-128 were consistent with previously reported data using ThT [21,44], suggesting that YAT2150 is a reliable tool for studying amyloid kinetics and inhibitors *in vitro,* maintaining fluorescence stability comparable to ThT over at least 72 hours (data not shown).

To further validate DP-128's inhibitory effect, Aβ40 aggregation in the absence and presence of the compound was assessed by quantifying the soluble protein fraction after 24 hours of incubation at 37ºC with 1200 rpm agitation. Following centrifugation and considering that 85-90% of the total Aβ40 peptide aggregates [45–47], absorbance at 280 nm revealed that 61% of the protein remained soluble in the presence of DP128. Direct visualization of amyloid fibrils and aggregates by AFM confirmed a considerable reduction in amyloid fibrils in the presence of DP-128, further supporting its inhibitory effect (**Figure 7**). These results align with YAT2150-based measurements, reinforcing its reliability in monitoring amyloid aggregation and inhibition.

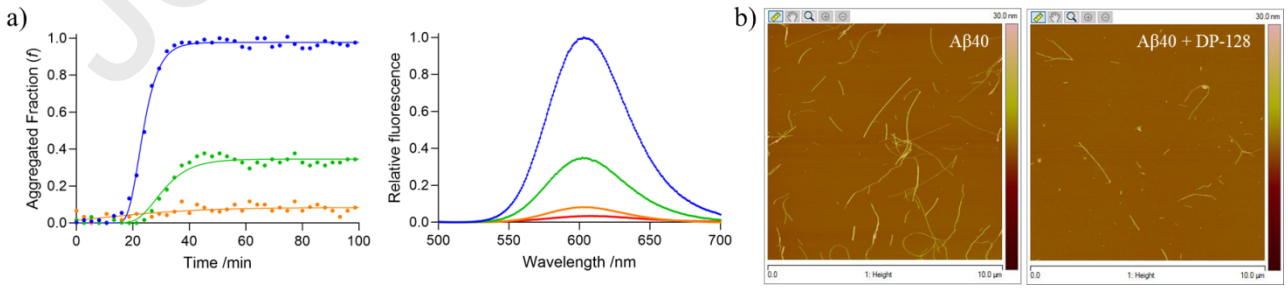

Figure 7. a) *In vitro* aggregation kinetics of Aβ40 peptide. Aβ40 in amyloid conformation was followed by the determination of YAT2150 fluorescence increase (left panel) and the end-time fluorescence spectrum (right

panel) in the absence (blue) and presence of DP-128 inhibitor at concentrations of 10 μM (green) and 100 μM (orange). In red, the negative control with YAT2150. b) AFM images of Aβ40 samples incubated in the absence (left) and presence (right) of DP-128.

The kinetics of amyloid aggregation follows an autocatalytic reaction model, as discussed in previous studies [29,48]. In this context, we studied the effect of the compound DP-128 at concentrations of 10 μM and 100 μM on the kinetics of the Aβ40 aggregation. In the presence of 10 μM DP-128, a significant decrease in the nucleation constant (k_n) was observed, from $4.08 \cdot 10^{-5}$ min^{-1} in the absence of the compound to $1.21 \cdot 10^{-6}$ min^{-1}, indicating a delay in the formation of the aggregation nucleus. This delay was also reflected in the lag time (t_0), which increased from 17.6 to 24.9 min. This suggests that DP-128 partially inhibits nucleation by delaying the formation of the first aggregates. Furthermore, the half-aggregation time ($t_{1/2}$) increased from 24.5 to 31.8 min, and the final aggregation time (t_1) was delayed from 31.5 to 38.7 min. Regarding the elongation constant (k_e), a slight increase was observed in the presence of DP-128, rising from 25620 $M^{-1} \cdot min^{-1}$ to 27033 $M^{-1} \cdot min^{-1}$. This suggests that DP-128 binds to Aβ40 monomers, preventing the formation of productive nuclei or hindering the development of on-pathway nuclei. However, once the initial productive nuclei are formed, fibril elongation follows a similar pattern as in the absence of the inhibitor, indicating that DP-128 does not affect fibril growth. In the presence of 100 μM DP-128, the inhibition is nearly total, and the kinetic parameters cannot be determined due to the near-absence of aggregate formation. Interestingly, in a previous study we conducted, the *in cellula* kinetics of Aβ40 aggregation was also analysed using ThS [13]. Despite the differences in experimental protocols, the observed trend was consistent with the results presented here, further supporting the inhibitory effect of DP-128 on Aβ40 aggregation and highlighting the value of YAT2150 in monitoring aggregation kinetics.

3.2. *In cellula* detection of inclusion bodies

3.2.1. *In cellula* detection of intracellular amyloid aggregates

Following the successful demonstration of YAT2150's capacity to bind to amyloid aggregates and monitor kinetics *in vitro*, further tests were conducted *in cellula* to assess its ability to detect intracellular protein aggregates (inclusion bodies, IBs). *In cellula* assays offer a more physiologically relevant environment, as they involve processes of protein synthesis, folding, and aggregation within cells, providing insight into how YAT2150 performs under more natural conditions compared to *in vitro* studies.

In this case, assays were performed using *E. coli* overexpressing amyloidogenic proteins. The proteins studied included Aβ42, α-SynH, HET-s PFD and Ure2p. Ure2p was included as a negative control since this protein is primarily produced natively in bacteria under our conditions (R.S. personal communication). YAT2150 was used at 2 µM, and tests were conducted up to 10 µM without detecting any adverse effect on bacterial growth (data not shown). The fluorescence ratio between induced cultures (overexpressing amyloid protein and forming IBs) and non-induced cultures (not forming IBs) was calculated for each protein tested in the presence of YAT2150 (**Table 1**). Our probe was compared with ThS as a reference for monitoring amyloid aggregation *in cellula* (**Table 2**) [13]. YAT2150 successfully distinguished amyloidogenic IBs from non-aggregating controls, with the fluorescence signal of *E. coli* cells expressing Aβ42, α-SynH, and HET-s PFD being 1.86, 1.85, and 1.42 times higher, respectively, than in non-induced cells. The difference for Ure2p, as expected, was negligible (1.08), indicating a weak binding of YAT2150 to the non-amyloid aggregates formed by this protein.

When comparing the staining activity of YAT2150 with that of ThS, and in agreement with *in vitro* results, YAT2150 was able to stain HET-s PFD aggregates ($p < 0.05$, HET-s PFD vs Ure2p) that ThS hardly detected ($p > 0.05$, HET-s PFD vs Ure2p), demonstrating that YAT2150 can detect intracellular amyloid aggregates even in cases where other dyes, like ThS, fail.

If considering the fluorescence of Aβ42 stained with YAT2150 (1.86) as the maximum fluorescence value, the ability of YAT2150 to detect α-SynH IBs was very similar (99.53%), while the detection of HET-s PFD IBs was around 50% (48.93%) (**Table 3**).

Table 1. YAT2150 fluorescence ratio between induced and non-induced *E. coli* cells expressing Aβ42, α-SynH, HET-s PFD and Ure2p.

Protein	Fluorescence ratio of YAT2150	SEM	SD
Aβ42	1.86*	0.02	0.05
α-SynH	1.85*	0.06	0.16
HET-s PFD	1.42*	0.04	0.13
Ure2p	1.08	0.04	0.11

* *p-value* < 0.05 vs Ure2p

Table 2. ThS fluorescence ratio between induced and non-induced *E. coli* cells expressing Aβ42, α-SynH, HET-s PFD and Ure2p.

Protein	ThS fluorescence ratio	SEM	SD
Aβ42	2.15*	0.96	0.04
α-SynH	1.48*	0.52	0.09
HET-s PFD	1.18	0.59	0.11
Ure2p	1.04	0.52	0.03

* *p-value* < 0.05 vs Ure2p

Table 3. IBs detection with YAT2150 in *E. coli* cells overexpressing amyloid-like proteins.

Protein	Relative fluorescence of YAT2150 (%)	SEM	SD
Aβ42	100	1.2	2.9
α-SynH	99.5	3.0	8.5
HET-s PFD	48.9	3.0	9.4
Ure2p	9.0	4.1	10.0

Confocal microscopy confirmed that YAT2150 can effectively penetrate bacterial cells, allowing for the staining of intracellular amyloid aggregates. In the micrographs (**Figure 7**), amyloid inclusion bodies (indicated by white arrows) are visible within *E. coli* cells overexpressing Aβ42 and HET-s PFD. Both YAT2150 and ThS exhibited stronger fluorescence at the cell poles, corresponding to regions of higher aggregate density. Similar to previous *in vitro* results, YAT2150 was able to stain inclusion bodies formed by HET-s PFD, offering a distinct advantage over ThS in amyloid detection within bacterial cells.

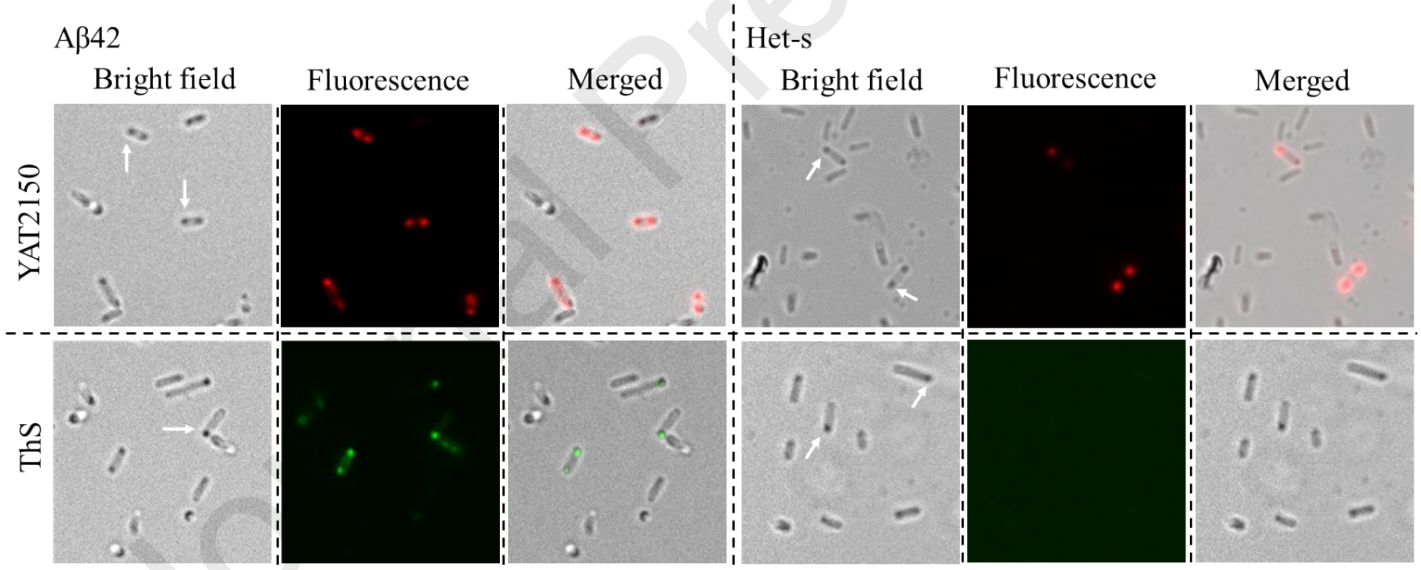

Figure 8. Confocal micrographs of *E. coli* cells overexpressing Aβ42 and HET-s PFD, and stained with YAT2150 and with ThS.

These results confirm that YAT2150 effectively detects intracellular amyloid aggregates in bacterial cells. While YAT2150 showed no effect on bacterial growth up to 10 μM, cytotoxicity assays in Neuro-2a cells (see Supplementary Figure S5) confirmed that, similarly to bacteria, it is well tolerated at concentrations up to 10 μM, supporting its suitability for mammalian cell studies. This

suggests that YAT2150 could also be used in eukaryotic cell models to investigate protein aggregation.

3.2.2. *In cellula* monitoring of amyloid aggregation kinetics and inhibition

The above assays demonstrated the applicability of YAT2150 to detect aggregates *in vitro* and *in cellula*, even those that thioflavins fail to detect. As a final step, we wanted to verify whether YAT2150 allows us to follow *in cellula* aggregation kinetics and thus be used as an alternative dye in our bacterial screening method for anti-amyloid compounds [49]. Results showed that incubating *E. coli* cells expressing Aβ42 with DP-128 amyloid inhibitor resulted in a significant decrease in YAT2150 fluorescence compared to cells induced without this compound (**Figure 9**). Notably, YAT2150 fluorescence remains stable for more than five days *in cellula*, reinforcing its reliability as a long-term aggregation marker in cellular environments (data not shown). The inhibition percentage was calculated by dividing the final fluorescence of the control (maximum aggregation without DP-128) by the final fluorescence of each aggregation inhibited with DP-128 at 5, 10 and 20 µM, obtaining inhibitions of 54.5%, 65.3% and 69.1%, respectively (**Table 4**).

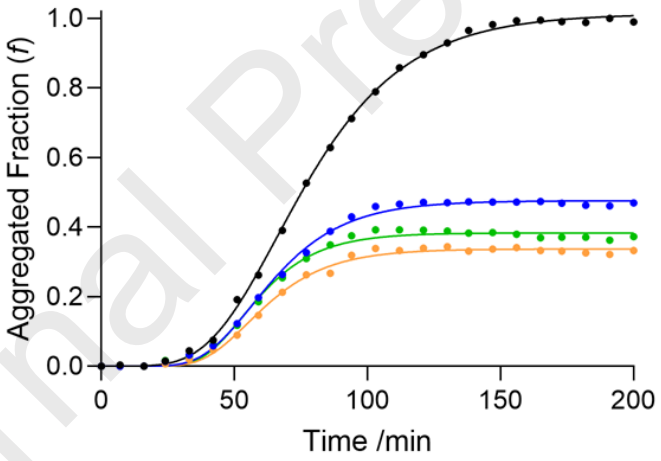

Figure 9. *In cellula* aggregation kinetics of Aβ42 peptide in the absence (black) and presence of the amyloid inhibitor DP-128 at 5 (blue), 10 (green) and 20 µM (orange), monitored by YAT2150.

Considering amyloid aggregation *in cellula* as an autocatalytic reaction [13], kinetic and thermodynamic parameters of Aβ42 aggregation were calculated (**Table 4**). Both the nucleation constant (k_n) and the apparent elongation constant (k_e^{app}) of Aβ42 showed a slight increase when aggregated in the presence of DP-128. The increase in nucleation and elongation rates translates into an acceleration of nuclei formation and fibril elongation, respectively, leading to a reduction of lag time (t_0), half-aggregation time ($t_{1/2}$) and end time (t_1). This phenomenon has previously been observed in other amyloid aggregation inhibitors [13,48]. The acceleration of aggregation in the early stages

may increase non-productive amorphous aggregates to the detriment of amyloid structures, thus causing a reduction in the final concentration of amyloid structures.

Table 4. Kinetic and thermodynamic parameters of Aβ42 aggregation.

[DP-128]	0 µM	5 µM	10 µM	20 µM
k_n (min^{-1})	$8.77x10^{-4}$	$9.85x10^{-4}$	$1.08x10^{-3}$	$1.10x10^{-3}$
k_e^{app} (M^{-1} min^{-1})[a]	8358.3	10863.3	11351.7	10930.0
t_0 (min)	38.0	31.7	32.9	32.4
$t_{1/2}$ (min)	79.0	64.6	60.9	62.0
t_1 (min)	120.0	97.5	88.8	91.5
Inhibition (%)	0.0	54.5	65.3	69.1

[a] To calculate k_e^{app}, a final concentration of Aβ42 of 6 µM was considered [13].

CONCLUSIONS

In vitro results demonstrated that YAT2150 effectively detects amyloid aggregates from different origins, including those of HET-s PFD not detectable using thioflavins. Moreover, YAT2150 can track amyloid aggregation kinetics, providing insights into the temporal progression of amyloid formation. *In cellula* assays using *E. coli* expressing different amyloidogenic proteins further confirmed that YAT2150 can detect intracellular aggregates, including those formed by HET-s PFD, supporting the *in vitro* results. These results highlight YAT2150's potential as a real-time monitoring tool for amyloid aggregation in live cells, as well as its utility for screening amyloid inhibitors in bacterial systems. The ability of YAT2150 to monitor kinetic changes in aggregation makes it a valuable asset for investigating both amyloid formation and inhibition. Such kinetic studies are essential in drug discovery efforts targeting amyloid-related diseases, where inhibitors must intervene early in aggregation. The inhibition data obtained with the amyloid inhibitor DP-128 align with previous findings using ThT, further validating YAT2150's reliability for studying amyloid kinetics and evaluating therapeutic agents.

In our model, YAT2150 was shown to detect amyloid-like IBs in living cells. Its superior performance over ThS in detecting HET-s PFD aggregates further emphasizes YAT2150's potential as a more reliable indicator of amyloid structures in complex cellular environments.

Practical applications of YAT2150 include drug discovery programs aimed at targeting intracellular amyloid formation. Its ability to monitor real-time aggregation in living cells offers valuable insights into the dynamics of amyloidogenesis. Additionally, its effectiveness in cells

expressing Aβ42 and α-SynH –proteins associated with Alzheimer's and Parkinson's disease, which together account for ~80% of global dementia cases and affect ~55 million people according to the World Health Organisation [50]– underscores its broader potential in studying aggregation processes in neurodegenerative diseases and evaluating the efficacy of aggregation inhibitors.

In conclusion, YAT2150 is a highly selective and versatile tool for studying protein aggregation mechanisms in amyloid-related diseases. It offers significant promise for the development of detection techniques for monitoring amyloid aggregation *in vivo*.

Data availability

The atomistic model of the binding mode of YAT2150 to the Aβ1-40 fibrils has been uploaded to a public repository (https://github.com/salomellabres/bm_yat2150).

CRediT authorship contribution statement

Irene Álvarez-Berbel: Formal analysis, investigation, methodology, writing-review & editing. **Salomé Llabrés**: Data curation, formal analysis, investigation, software, writing-review & editing. **Òscar Domènech**: Data curation, formal analysis, investigation, writing-review & editing. **Maria Antonia Busquets**: Formal analysis, methodology, project administration, writing-review & editing. **Xavier Fernàndez-Busquets**: Validation, writing-review & editing. **Elsa M. Arce**: Methodology, validation, writing-review & editing. **Rosalina Gavín**: Methodology, validation, writing-review & editing. **José Antonio del Río**: Methodology, validation, writing-review & editing. **Diego Muñoz-Torrero**: Methodology, validation, writing-review & editing. **F Javier Luque**: Data curation, formal analysis, methodology, software, validation, writing-review & editing. **Raimon Sabate**: Conceptualization, data curation, formal analysis, methodology, project administration, supervision, validation, writing-original draft, writing-review & editing. **Alba Espargaró**: Conceptualization, data curation, formal analysis, methodology, project administration, supervision, validation, writing-original draft, writing-review & editing.

Funding

This work was supported by grants (i) PID2021-127863OB-I00 (RS and AE), PID2021-127693OB-100, PID2023-147004OB-I00 (DM-T); PID2021-128325OB-I00 and PDC2022-133085-I00 (XF-B); and PID2021-123714OB-I00, PLEC2022-009401, PDC2022-133268-I00, and PID2024-162521OB-I00

(JAR and RG) funded by *Ministerio de Ciencia, Innovación y Universidades/Agencia Estatal de Investigación* (MCIU/AEI/ 10.13039/501100011033), which included FEDER and European Union NextGenerationEU/PRTR funds; and (ii) *Generalitat de Catalunya*, Spain (http://agaur.gencat.cat/), grant numbers 2021SGR00357 (DM-T), 2021SGR00635 (XF-B) and 2021SGR00671(SL and FJL), and SGR2021-00453 (JAR and RG) and the Consorci de Serveis Universitaris de Catalunya (CSUC, project Reconeixement Molecular,) for supercomputation resources (SL and FJL). ISGlobal and IBEC are members of the CERCA Programme, *Generalitat de Catalunya*. We acknowledge support from MCIN/AEI through the *"Centro de Excelencia Severo Ochoa 2019-2023"* Program (CEX2018-000806-S). This research is part of ISGlobal's Program on the Molecular Mechanisms of Malaria which is partially supported by the *Fundación Ramón Areces*.

Conflicts of Interest

The authors declare no conflicts of interest.

REFERENCE

[1] Chiti F, Dobson CM. Protein Misfolding, Amyloid Formation, and Human Disease: A Summary of Progress Over the Last Decade. Annu Rev Biochem 2017;86:27–68. https://doi.org/10.1146/annurev-biochem-061516-045115.

[2] Luheshi LM, Tartaglia GG, Brorsson A-C, Pawar AP, Watson IE, Chiti F, et al. Systematic In Vivo Analysis of the Intrinsic Determinants of Amyloid β Pathogenicity. PLoS Biol 2007;5:e290. https://doi.org/10.1371/journal.pbio.0050290.

[3] Espargaró A, Llabrés S, Saupe SJ, Curutchet C, Luque FJ, Sabaté R. On the Binding of Congo Red to Amyloid Fibrils. Angew Chem Int Ed 2020;59:8104–7. https://doi.org/10.1002/anie.201916630.

[4] Biancalana M, Koide S. Molecular mechanism of Thioflavin-T binding to amyloid fibrils. Biochim Biophys Acta 2010;1804:1405–12. https://doi.org/10.1016/j.bbapap.2010.04.001.

[5] Espargaró A, Sabate R, Ventura S. Thioflavin-S staining coupled to flow cytometry. A screening tool to detect in vivo protein aggregation. Mol Biosyst 2012;8:2839. https://doi.org/10.1039/c2mb25214g.

[6] Frid P, Anisimov S V., Popovic N. Congo red and protein aggregation in neurodegenerative diseases. Brain Res Rev 2007;53:135–60. https://doi.org/10.1016/j.brainresrev.2006.08.001.

[7] Hudson SA, Ecroyd H, Kee TW, Carver JA. The thioflavin T fluorescence assay for amyloid fibril detection can be biased by the presence of exogenous compounds. FEBS J 2009;276:5960–72. https://doi.org/10.1111/j.1742-4658.2009.07307.x.

[8] Patton WF, Yarmoluk SM, Pande P, Kovalska V, Dai L, Volkova K, et al. Dyes for analysis of protein aggregation. Patent application number: PCT/US20 10/003061. Patent number: WO2011/065980 A2. Date filed: 30–11–2010. Date issued: 3–6–2011.

[9] Navarro S, Ventura S. Fluorescent dye ProteoStat to detect and discriminate intracellular amyloid-like aggregates in Escherichia coli. Biotechnol J 2014;9:1259–66. https://doi.org/10.1002/biot.201400291.

[10] Sabaté R, Ventura S. Cross-β-Sheet Supersecondary Structure in Amyloid Folds: Techniques for Detection and Characterization. Methods Mol Biol 2012;932:237–57. https://doi.org/10.1007/978-1-62703-065-6_15.

[11] Villar-Pique A, Espargaro A, Ventura S, Sabate R. Screening for Amyloid Aggregation: In-Silico, In-Vitro and In-Vivo Detection. Curr Protein Pept Sci 2014;15:477–89. https://doi.org/10.2174/1389203715666140221101038.

[12] Navarro S, Carija A, Muñoz-Torrero D, Ventura S. A fast and specific method to screen for intracellular amyloid inhibitors using bacterial model systems. Eur J Med Chem 2016;121:785–92. https://doi.org/10.1016/j.ejmech.2015.10.044.

[13] Espargaró A, Medina A, Di Pietro O, Muñoz-Torrero D, Sabate R. Ultra rapid in vivo screening for anti-Alzheimer anti-amyloid drugs. Sci Rep 2016;6:23349. https://doi.org/10.1038/srep23349.

[14] Rosano GL, Ceccarelli EA. Recombinant protein expression in Escherichia coli: advances and challenges. Front Microbiol 2014;5:172. https://doi.org/10.3389/fmicb.2014.00172.

[15] Sabate R, de Groot NS, Ventura S. Protein folding and aggregation in bacteria. Cell Mol Life Sci 2010;67:2695–715. https://doi.org/10.1007/s00018-010-0344-4.

[16] Wang L, Maji SK, Sawaya MR, Eisenberg D, Riek R. Bacterial Inclusion Bodies Contain Amyloid-Like Structure. PLoS Biol 2008;6:e195. https://doi.org/10.1371/journal.pbio.0060195.

[17] Morell M, Bravo R, Espargaró A, Sisquella X, Avilés FX, Fernàndez-Busquets X, et al. Inclusion bodies: Specificity in their aggregation process and amyloid-like structure. Biochim Biophys Acta 2008;1783:1815–25. https://doi.org/10.1016/j.bbamcr.2008.06.007.

[18] Caballero AB, Gamez P, Sabate R, Espargaró A. Anti-Amyloid Drug Screening Methods Using Bacterial Inclusion Bodies. Methods Mol Biol 2022;2538:165–88. https://doi.org/10.1007/978-1-0716-2529-3_12.

[19] Wasmer C, Benkemoun L, Sabaté R, Steinmetz MO, Coulary-Salin B, Wang L, et al. Solid-State NMR Spectroscopy Reveals that E. coli Inclusion Bodies of HET-s(218 - 289) are Amyloids. Angew Chem Int Ed 2009;48:4858–60. https://doi.org/10.1002/anie.200806100.

[20] Espargaró A, Ginex T, Vadell M del M, Busquets MA, Estelrich J, Muñoz-Torrero D, et al. Combined in Vitro Cell-Based/in Silico Screening of Naturally Occurring Flavonoids and

Phenolic Compounds as Potential Anti-Alzheimer Drugs. J Nat Prod 2017;80:278–89. https://doi.org/10.1021/ACS.JNATPROD.6B00643/SUPPL_FILE/NP6B00643_SI_001.PDF.

[21] Di Pietro O, Pérez-Areales FJ, Juárez-Jiménez J, Espargaró A, Clos MV, Pérez B, et al. Tetrahydrobenzo[h][1,6]naphthyridine-6-chlorotacrine hybrids as a new family of anti-Alzheimer agents targeting β-amyloid, tau, and cholinesterase pathologies. Eur J Med Chem 2014;84:107–17. https://doi.org/10.1016/j.ejmech.2014.07.021.

[22] Sabaté R, Baxa U, Benkemoun L, Sánchez de Groot N, Coulary-Salin B, Maddelein M, et al. Prion and Non-prion Amyloids of the HET-s Prion forming Domain. J Mol Biol 2007;370:768–83. https://doi.org/10.1016/j.jmb.2007.05.014.

[23] Sabaté R, Villar-Piqué A, Espargaró A, Ventura S. Temperature Dependence of the Aggregation Kinetics of Sup35 and Ure2p Yeast Prions. Biomacromolecules 2012;13:474–83. https://doi.org/10.1021/bm201527m.

[24] Rezaei H, Marc D, Choiset Y, Takahashi M, Hui Bon Hoa G, Haertlé T, et al. High yield purification and physico-chemical properties of full-length recombinant allelic variants of sheep prion protein linked to scrapie susceptibility. Eur J Biochem 2000;267:2833–9. https://doi.org/10.1046/j.1432-1033.2000.01347.x.

[25] Sabaté R, Espargaró A, de Groot NS, Valle-Delgado JJ, Fernàndez-Busquets X, Ventura S. The Role of Protein Sequence and Amino Acid Composition in Amyloid Formation: Scrambling and Backward Reading of IAPP Amyloid Fibrils. J Mol Biol 2010;404:337–52. https://doi.org/10.1016/j.jmb.2010.09.052.

[26] Holm NK, Jespersen SK, Thomassen L V., Wolff TY, Sehgal P, Thomsen LA, et al. Aggregation and fibrillation of bovine serum albumin. Biochim Biophys Acta 2007;1774:1128–38. https://doi.org/10.1016/j.bbapap.2007.06.008.

[27] Frare E, Polverino de Laureto P, Zurdo J, Dobson CM, Fontana A. A Highly Amyloidogenic Region of Hen Lysozyme. J Mol Biol 2004;340:1153–65. https://doi.org/10.1016/j.jmb.2004.05.056.

[28] Gancar M, Kurin E, Bednarikova Z, Marek J, Mucaji P, Nagy M, et al. Amyloid Aggregation of Insulin: An Interaction Study of Green Tea Constituents. Sci Rep 2020;10:9115. https://doi.org/10.1038/s41598-020-66033-6.

[29] Sabaté R, Gallardo M, Estelrich J. An autocatalytic reaction as a model for the kinetics of the aggregation of β-amyloid. Biopolymers 2003;71:190–5. https://doi.org/10.1002/bip.10441.

[30] Ghosh U, Thurber KR, Yau W-M, Tycko R. Molecular structure of a prevalent amyloid-β fibril polymorph from Alzheimer's disease brain tissue. Proc Natl Acad Sci USA 2021;118:e2023089118. https://doi.org/10.1073/pnas.2023089118.

[31] Olsson MHM, Søndergaard CR, Rostkowski M, Jensen JH. PROPKA3: Consistent Treatment of Internal and Surface Residues in Empirical pKa Predictions. J Chem Theory Comput 2011;7:525–37. https://doi.org/10.1021/ct100578z.

[32] Ruiz-Carmona S, Alvarez-Garcia D, Foloppe N, Garmendia-Doval AB, Juhos S, Schmidtke P, et al. rDock: A Fast, Versatile and Open Source Program for Docking Ligands to Proteins and Nucleic Acids. PLoS Comput Biol 2014;10:e1003571. https://doi.org/10.1371/journal.pcbi.1003571.

[33] Maier JA, Martinez C, Kasavajhala K, Wickstrom L, Hauser KE, Simmerling C. ff14SB: Improving the Accuracy of Protein Side Chain and Backbone Parameters from ff99SB. J Chem Theory Comput 2015;11:3696–713. https://doi.org/10.1021/acs.jctc.5b00255.

[34] Joung IS, Cheatham TE. Determination of Alkali and Halide Monovalent Ion Parameters for Use in Explicitly Solvated Biomolecular Simulations. J Phys Chem B 2008;112:9020–41. https://doi.org/10.1021/jp8001614.

[35] Mark P, Nilsson L. Structure and Dynamics of the TIP3P, SPC, and SPC/E Water Models at 298 K. J Phys Chem A 2001;105:9954–60. https://doi.org/10.1021/jp003020w.

[36] Gaussian 09, Revision A.02, M. J. Frisch, G. W. Trucks, H. B. Schlegel, G. E. Scuseria, M. A. Robb, J. R. Cheeseman, G. Scalmani, V. Barone, G. A. Petersson, H. Nakatsuji, X. Li, M. Caricato, A. Marenich, J. Bloino, B. G. Janesko, R. Gomperts, B. Mennucci, H. P. Hratchian, J. V. Ortiz, A. F. Izmaylov, J. L. Sonnenberg, D. Williams-Young, F. Ding, F. Lipparini, F. Egidi, J. Goings, B. Peng, A. Petrone, T. Henderson, D. Ranasinghe, V. G. Zakrzewski, J. Gao, N. Rega, G. Zheng, W. Liang, M. Hada, M. Ehara, K. Toyota, R. Fukuda, J. Hasegawa, M. Ishida, T. Nakajima, Y. Honda, O. Kitao, H. Nakai, T. Vreven, K. Throssell, J. A. Montgomery, Jr., J. E. Peralta, F. Ogliaro, M. Bearpark, J. J. Heyd, E. Brothers, K. N. Kudin, V. N. Staroverov, T. Keith, R. Kobayashi, J. Normand, K. Raghavachari, A. Rendell, J. C. Burant, S. S. Iyengar, J. Tomasi, M. Cossi, J. M. Millam, M. Klene, C. Adamo, R. Cammi, J. W. Ochterski, R. L. Martin, K. Morokuma, O. Farkas, J. B. Foresman, and D. J. Fox, Gaussian, Inc., Wallingford CT, 2016.

[37] D.A. Case, H.M. Aktulga, K. Belfon, I.Y. Ben-Shalom, J.T. Berryman, S.R. Brozell, D.S. Cerutti, T.E. Cheatham, III, G.A. Cisneros, V.W.D. Cruzeiro, T.A. Darden, N. Forouzesh, M. Ghazimirsaeed, G. Giambaşu, T. Giese, M.K. Gilson, H. Gohlke, A.W. Goetz, J. Harris, Z. Huang, S. Izadi, S.A. Izmailov, K. Kasavajhala, M.C. Kaymak, A. Kovalenko, T. Kurtzman, T.S. Lee, P. Li, Z. Li, C. Lin, J. Liu, T. Luchko, R. Luo, M. Machado, M. Manathunga, K.M. Merz, Y. Miao, O. Mikhailovskii, G. Monard, H. Nguyen, K.A. O'Hearn, A. Onufriev, F. Pan, S. Pantano, A. Rahnamoun, D.R. Roe, A. Roitberg, C. Sagui, S. Schott-Verdugo, A. Shajan, J. Shen, C.L. Simmerling, N.R. Skrynnikov, J. Smith, J. Swails, R.C. Walker, J. Wang, J. Wang, X. Wu, Y. Wu, Y. Xiong, Y. Xue, D.M. York, C. Zhao, Q. Zhu, and P.A. Kollman (2024), Amber 2024, University of California, San Francisco.

[38] Sabate R, Rodriguez-Santiago L, Sodupe M, Saupe SJ, Ventura S. Thioflavin-T excimer formation upon interaction with amyloid fibers. Chem Commun 2013;49:5745-7. https://doi.org/10.1039/c3cc42040j.

[39] Vázquez G, Espargaró A, Caballero AB, Di Pede-Mattatelli A, Busquets MA, Nawrot D, et al. A versatile luminescent probe for sensing and monitoring amyloid proteins. Dyes Pigments 2024;231:112348. https://doi.org/10.1016/j.dyepig.2024.112348.

[40] Fu Z, Crooks EJ, Irizarry BA, Zhu X, Chowdhury S, Van Nostrand WE, et al. An electrostatic cluster guides Aβ40 fibril formation in sporadic and Dutch-type cerebral amyloid angiopathy. J Struct Biol 2024;216:108092. https://doi.org/10.1016/j.jsb.2024.108092.

[41] Pfeiffer PB, Ugrina M, Schwierz N, Sigurdson CJ, Schmidt M, Fändrich M. Cryo-EM Analysis of the Effect of Seeding with Brain-derived Aβ Amyloid Fibrils. J Mol Biol 2024;436:168422. https://doi.org/10.1016/j.jmb.2023.168422.

[42] Frieg B, Han M, Giller K, Dienemann C, Riedel D, Becker S, et al. Cryo-EM structures of lipidic fibrils of amyloid-β (1-40). Nat Commun 2024;15:1297. https://doi.org/10.1038/s41467-023-43822-x.

[43] Shen D, Coleman J, Chan E, Nicholson TP, Dai L, Sheppard PW, et al. Novel Cell- and Tissue-Based Assays for Detecting Misfolded and Aggregated Protein Accumulation Within Aggresomes and Inclusion Bodies. Cell Biochem Biophys 2011;60:173–85. https://doi.org/10.1007/s12013-010-9138-4.

[44] Espargaró A, Pont C, Gamez P, Muñoz-Torrero D, Sabate R. Amyloid Pan-inhibitors: One Family of Compounds to Cope with All Conformational Diseases. ACS Chem Neurosci 2019;10:1311–7. https://doi.org/10.1021/acschemneuro.8b00398.

[45] Sabaté R, Estelrich J. Pinacyanol as effective probe of fibrillar β-amyloid peptide: Comparative study with Congo Red. Biopolymers 2003;72:455–63. https://doi.org/10.1002/bip.10485.

[46] Hasegawa K, Yamaguchi I, Omata S, Gejyo F, Naiki H. Interaction between Aβ(1−42) and Aβ(1−40) in Alzheimer's β-Amyloid Fibril Formation in Vitro. Biochemistry 1999;38:15514–21. https://doi.org/10.1021/bi991161m.

[47] Chauhan VPS, Chauhan A, Wegiel J. Fibrillar amyloid β-protein forms a membrane-like hydrophobic domain. Neuroreport 2001;12:587–90.

[48] Kowalczyk J, Grapsi E, Espargaró A, Caballero AB, Juárez-Jiménez J, Busquets MA, et al. Dual Effect of Prussian Blue Nanoparticles on Aβ40 Aggregation: β-Sheet Fibril Reduction and Copper Dyshomeostasis Regulation. Biomacromolecules 2021;22:430–40. https://doi.org/10.1021/acs.biomac.0c01290.

[49] Pouplana S, Espargaró A, Galdeano C, Viayna E, Sola I, Ventura S, et al. Thioflavin-S Staining of Bacterial Inclusion Bodies for the Fast, Simple, and Inexpensive Screening of Amyloid Aggregation Inhibitors. Curr Med Chem 2014;21:1152–9.

[50] World Health Organization. Dementia. Accessed 27 December 2024. https://www.who.int/news-room/fact-sheets/detail/dementia

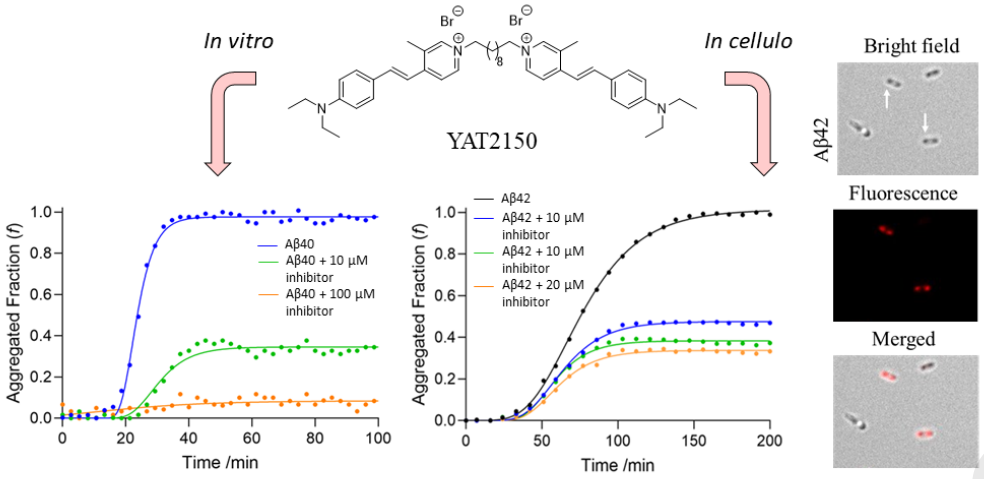

Declaration of interests

☒ The authors declare that they have no known competing financial interests or personal relationships that could have appeared to influence the work reported in this paper.

☐ The authors declare the following financial interests/personal relationships which may be considered as potential competing interests: